Load-Dependent Assembly of the Bacterial Flagellar Motor

Murray J. Tipping, Nicolas J. Delalez, Ren Lim, et al.
**2013. Load-Dependent Assembly of the Bacterial Flagellar Motor . mBio 4(4): .
doi:10.1128/mBio.00551-13.**

Load-Dependent Assembly of the Bacterial Flagellar Motor

Murray J. Tipping,[a]* Nicolas J. Delalez,[a] Ren Lim,[b] Richard M. Berry,[b] Judith P. Armitage[a]

Department of Biochemistry, University of Oxford, Oxford, United Kingdom[a]; Clarendon Laboratory, Department of Physics, Oxford, United Kingdom[b]

* Present address: Department of Molecular and Cellular Biology, Harvard University, Cambridge, Massachusetts, USA.

ABSTRACT **It is becoming clear that the bacterial flagellar motor output is important not only for bacterial locomotion but also for mediating the transition from liquid to surface living. The output of the flagellar motor changes with the mechanical load placed on it by the external environment: at a higher load, the motor runs more slowly and produces higher torque. Here we show that the number of torque-generating units bound to the flagellar motor also depends on the external mechanical load, with fewer stators at lower loads. Stalled motors contained at least as many stators as rotating motors at high load, indicating that rotation is unnecessary for stator binding. Mutant stators incapable of generating torque could not be detected around the motor. We speculate that a component of the bacterial flagellar motor senses external load and mediates the strength of stator binding to the rest of the motor.**

IMPORTANCE **The transition between liquid living and surface living is important in the life cycles of many bacteria. In this paper, we describe how the flagellar motor, used by bacteria for locomotion through liquid media and across solid surfaces, is capable of adjusting the number of bound stator units to better suit the external load conditions. By stalling motors using external magnetic fields, we also show that rotation is not required for maintenance of stators around the motor; instead, torque production is the essential factor for motor stability. These new results, in addition to previous data, lead us to hypothesize that the motor stators function as mechanosensors as well as functioning as torque-generating units.**

Received 22 July 2013 **Accepted** 23 July 2013 **Published** 20 August 2013

Citation Tipping MJ, Delalez NJ, Lim R, Berry RM, Armitage JP. 2013. Load-dependent assembly of the bacterial flagellar motor. mBio 4(4):e00551-13. doi:10.1128/mBio.00551-13.

Editor Bonnie Bassler, Princeton University

Address correspondence to Judith P. Armitage, judith.armitage@bioch.ox.ac.uk.

Many bacterial species swim, driven by transmembrane molecular motors rotating extracellular flagellar filaments. In some species, for example, *Salmonella*, motor rotation is required both for swimming through liquid media (1) and for swarming across solid surfaces (2). Flagellar motors contain a series of rotating protein rings (3). A schematic of the *Escherichia coli* flagellar motor can be seen in Fig. 1a. The C-ring, also called the switch complex, is made of 26 or more copies of FliG, 34 to 35 of FliM, and ~140 of FliN. The C-ring connects via the transmembrane rod to the extracellular flagellar filament and interacts with cell wall-anchored transmembrane stator complexes formed by the proteins MotA and MotB. *E. coli* motors are bidirectional: motors can switch between counterclockwise (CCW) and clockwise (CW) rotation in response to chemosensory signals, with switching transmitted through C-ring proteins FliM and FliN on the cytoplasmic side of FliG.

E. coli motors have been shown to be dynamic rather than stable structures, with protein components exchanging between working motors and cellular pools of "spares" in response to different intra- and extracellular signals. The stator protein MotB in *E. coli*, labeled with green fluorescent protein (GFP-MotB), was the first shown to exchange. Each GFP-MotB molecule remained bound to the motor for an average of only 30 s (4). The rotor protein FliM also exchanges on a slightly longer time scale but only in the presence of the switch regulator CheY (5). FliM exchange has been explained as part of a mechanism of adaptation of the motor switch to variations in the concentrations of chemotaxis proteins, allowing motors to remain in the hypersensitive switching range of their response curve to the CheY concentration (6).

The stability of stator binding to the flagellar motor depends upon the ion-motive force (IMF) that drives flagellar rotation. Stators leave both Na^+- and H^+-driven motors when IMF is disrupted and return after IMF restoration (7–9). The mechanism for this process is unknown. Removing the IMF stops both torque and rotation of the motor, and either could be the direct trigger for stator loss.

There can be at least 11 stators associated with a rotor, but it is also known that at low loads a single stator can rotate the *E. coli* motor at full speed (10). Here we show that reducing the load reduces the number of stators in a motor and therefore presumably their binding affinity for the motor. In contrast, motors that were stalled for up to 300 s still contained the maximum number of stators. These results support the hypothesis that torque, but not rotation, is necessary for stators to bind stably to the motor, allowing motors to change the number of bound stators to suit their environment.

RESULTS

Correlation between stator number and motor speed at high load. Although a maximum of ~11 stators are thought to be able

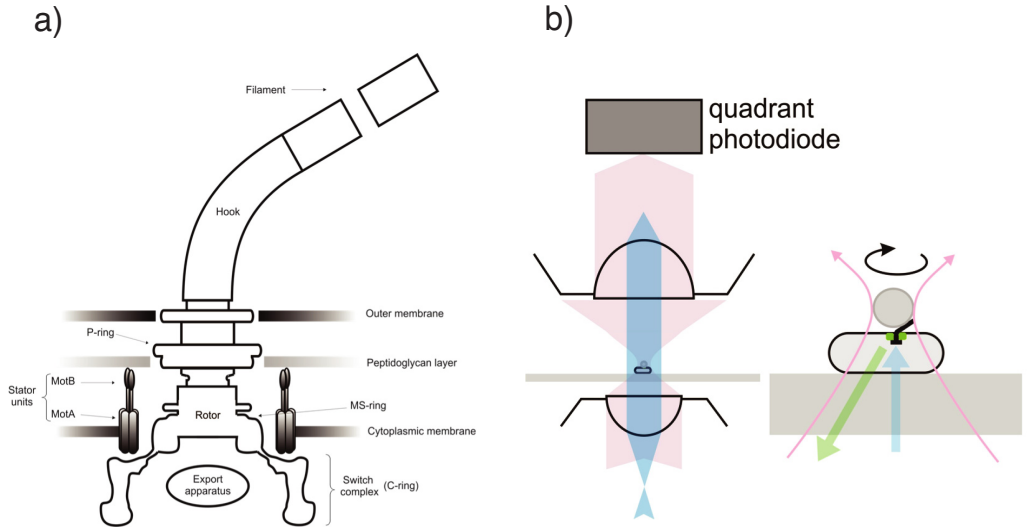

FIG 1 (A) A schematic of the *E. coli* flagellar motor. Torque is generated by ion flow through the membrane bound stator units, causing rotation of the rotor, hook and flagellar filament. (B) A schematic of the apparatus used for simultaneous speed/fluorescence measurements. Cells were immobilised on glass surfaces, and beads attached to exposed flagellar filament stubs. Bead movement was measured through the quadrant photodiode signal from a 1064 nm laser (red), while epifluorescence measurements were taken of the motor spot (excitation in blue, emission in green). In experiments with magnetic beads, motors could be stalled by addition of a linear magnetic field with field lines parallel to the coverslip (see text for details).

to bind to the *E. coli* flagellar motor at high load, the transient nature of stator binding (4, 9) means that not all binding sites are necessarily occupied at any given time, even under high-load conditions. We investigated the relationship between motor speed and the number of stators bound to a functioning flagellar motor. Previous "resurrection" studies have shown that stator binding results in an increase in speed, but those experiments do not rule out the possibility of a semistable "bound but inactive" state for stators (10).

We measured the fluorescence intensity of motor spots in functioning motors while simultaneously measuring motor speed by monitoring the rotation of attached polystyrene beads. A schematic of the experiment can be seen in Fig. 1b. Figure 2a shows the mean intensity of GFP-MotB spots localized to functioning motors, each driving a 1-μm-diameter bead attached to the filament stub (high load), versus the simultaneously measured motor speed. Spot intensity was measured by epifluorescence microscopy using constant illumination intensity and exposure time, allowing direct comparison of relative motor spot intensities, and was normalized by dividing by the intensity of the fastest motor measured.

The intensity of each motor spot is proportional to the number of GFP-tagged MotB molecules in the motor (4). Thus, a straight line through the origin in Fig. 2a would indicate direct propor-

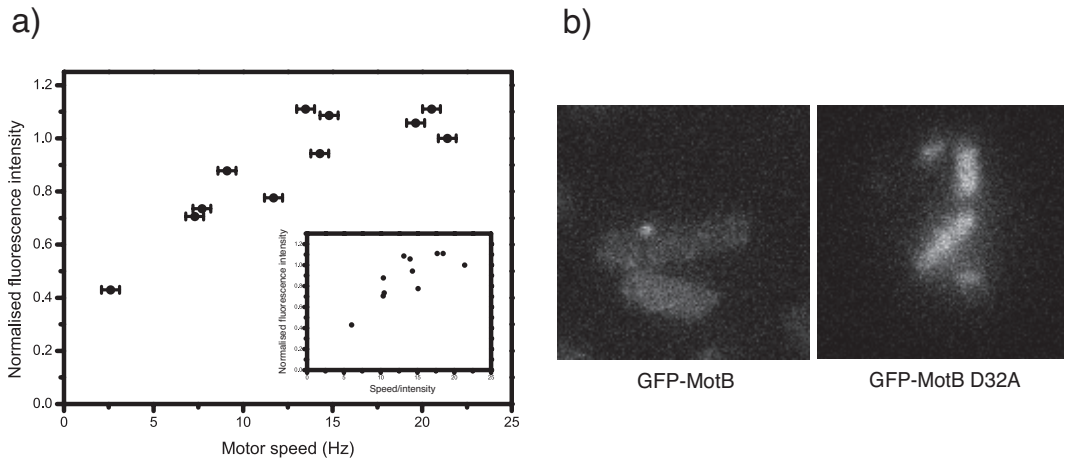

FIG 2 (A) A graph showing fluorescence intensity of GFP-MotB spots in 12 different motors from *E. coli* strain JPA806, plotted against simultaneously measured motor speed. Motors in all cases were driving a 1 μm bead attached to the flagellar filament stub. A direct relationship between speed and fluorescence intensity is observable, indicating increased stator number at higher speeds under these conditions. Error bars represent experimental error in speed measurements. The inset shows fluorescence intensity graphed against speed/intensity. (B) Two representative images of cells with attached 1 μm polystyrene beads from strain JPA806 (left), expressing GFP-MotB, and JPA807 (right), expressing the non-functional mutant protein GFP-MotB D32A. No fluorescence spot formation was visible in JPA807 cells.

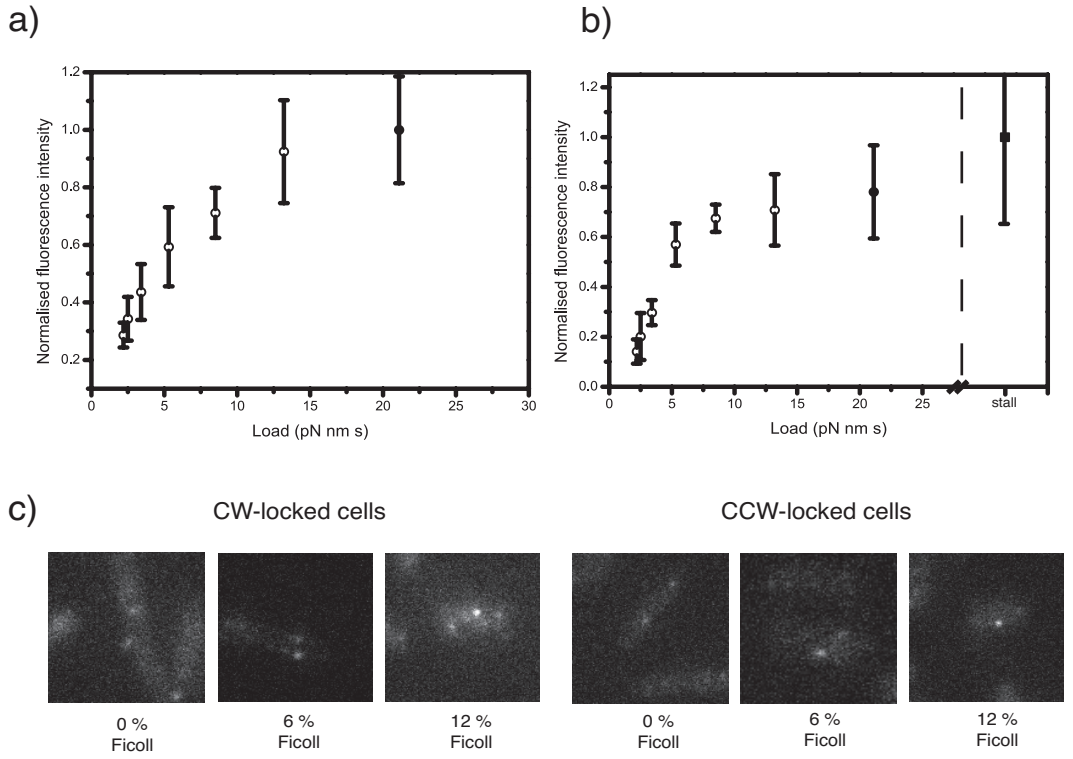

FIG 3 Fluorescence spot intensity plotted against external load for (A) CW-locked and (B) CCW-locked motors in *E. coli* strain JPA806. The load conditions shown are, in left-to-right order: 0.35 μm beads in 0, 1, 3, 6, 9 and 12% Ficoll (light circles) and 1μm beads with no Ficoll (filled circle), and, for the CCW graph, motors stalled by external magnetic fields (filled square). Each data point for rotating beads represents the mean fluorescence intensity of at least 15 motors for each load condition. 5 motors were measured for the stall data point. Error bars show s.d. of fluorescence intensities. Figure 4c shows representative fluorescence images of GFP-MotB spots in CW-locked (left) and CCW-locked (right) motors driving 0.35 μm beads through 0%, 6% and 12% Ficoll solutions.

tionality between stator number and speed, which would be expected if all stators in all motors measured generated the same torque. However, data points lie above this line, suggesting that other factors such as reduced IMFs or longer flagellar filament stubs may also contribute to lowered motor speeds. The previously observed dependence of stator binding on IMF may also explain why some motors have fewer stators than others: the data points toward the left in Fig. 2a would then correspond to motors with fewer stators and less speed per stator, both of which could be the consequence of lower IMF. The speed per stator at high load is proportional to IMF (11), and with spot intensity as a proxy for stator number, plotting spot intensity versus speed/intensity (Fig. 2a, inset) provides an indication of the possible dependence of stator number on IMF.

Regardless of these subtleties, slower motors were generally less fluorescent. This demonstrates both that fluorescence measurements can distinguish between different numbers of bound stators in functioning motors and that inactive or nonfunctional stators do not stably bind to the motor. The variability in stator number under high load is consistent with continuous stator exchange, leading to some motors having less than the maximum number of stators at any given time.

To further test the hypothesis that nonfunctional stators do not bind stably, we mutated chromosomal *gfp-motB* to express a D32A variant incapable of generating torque (12) and measured stator localization in the resulting *E. coli* strain (JPA807). Figure 2b shows representative fluorescence images of JPA806 (functional stators) and JPA807 cells with 1-μm-diameter polystyrene beads attached to flagellar filament stubs. We saw no fluorescent spots or bead rotation in 20 cells expressing GFP-MotB/D32A, whereas with functional GFP-MotB, fluorescent spots were observed in >95% of cells with rotating beads. This is consistent with a previous observation that the equivalent mutation in PomB, the homologue of MotB in Na^+-driven motors of *Vibrio alginolyticus*, showed very few fluorescent motor spots compared to the results seen with the functional protein (13).

Stator number varies with external load and motor direction. We measured the effects of load on stator number in functioning flagellar motors. Because observed torque-speed curves are different in CW- and CCW-locked motors (14), we repeated the experiment in both CW- and CCW-locked cells. Figure 3a and b show mean motor spot intensity in CW- and CCW-locked flagellar motors subjected to different viscous loads. Motors were CW locked by induced expression of the constitutively active CheY mutant variant CheY** (15) from plasmid pIND-CheY**. Without this plasmid, cells lacked CheY and were CCW locked. A total of 15 to 25 cells were measured for each load condition except for stalling, where 5 cells were measured. In most cases, external load was adjusted by addition of Ficoll to the motility medium, with motors rotating a 0.35-μm-diameter polystyrene bead. This provided a range of viscous drag coefficients of from 2.1 to 13.2 pN·nm·s (Fig. 3a and b, open circles). Additionally, to control

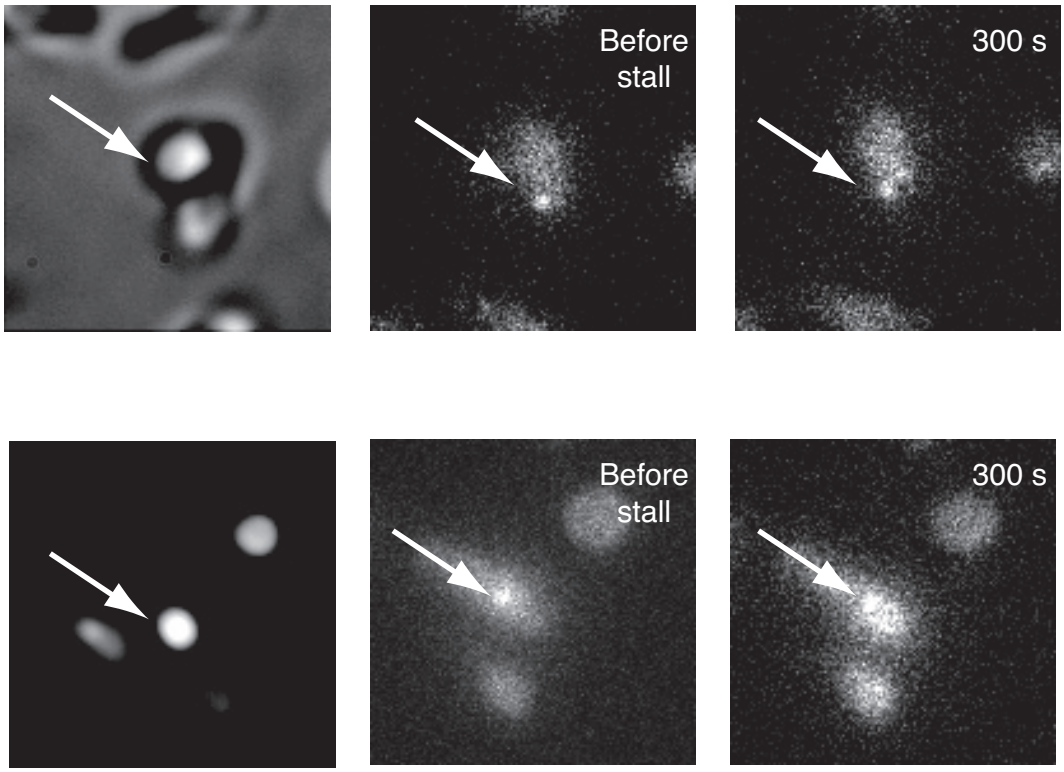

FIG 4 Representative time-course images of motors driving 1.0 μm magnetic SiO_2 beads during stall events. Motors were allowed to rotate freely (left and middle) before being subjected to a stall lasting 300 s (right) through application of an external magnetic field. No spot dissipation was observed during or after stall events.

for possible direct effects of Ficoll, spot intensities in motors driving 1.0-μm-diameter beads without Ficoll were used for the highest load measured in rotating cells (21 pN·nm·s) (Fig. 3a and b, filled circles). These experiments were a repeat of those described for Fig. 3 but without the infrared laser previously used for speed measurement. Fluorescent spots corresponding to stalled CCW-locked motors were also observed (Fig. 3b, filled square; see also Fig. 4). Fluorescence intensities were normalized to the value found for stalled cells, after correcting for the different illumination intensities, as these had the highest fluorescence. Figure 3c shows representative images of motor spots in cells subjected to high, intermediate, and low load conditions. Spot brightness, and thus stator number, increased monotonically with increasing load in both CCW- and CW-locked motors. The CCW spot brightness-versus-load curve shows a discontinuity at intermediate load similar to the "knee" that is seen in the torque-speed curve of CCW but not CW motors (7, 13). However, this difference is close to the limit of experimental uncertainty and should therefore be treated with caution.

Motor rotation is not required for stators to bind to the motor. We examined the response of motors to enforced motor stops by applying an external torque sufficient to stall the motor via the use of 1-μm-diameter magnetic S_1O_2 beads bound to biotinylated flagellar filament stubs (see Materials and Methods). In the absence of an external magnetic field, motors rotated as before, with the external load provided only by the viscous drag on the attached bead. Application of a linear magnetic field of 20 to 30 mT was sufficient to overcome the motor torque, causing motors to stall within $<$1 s as beads aligned with the magnetic field. Motor spot brightness was measured before stall and after 300 s of stall. When the magnets were subsequently removed, motors rotated freely again. Brightness measurements for cells before and after stall are shown (Table 1). Representative images of two cells can be seen in Fig. 4. In all cases, motor spots were at least as bright after 300 s of stall as before the stall. The results showed that 3 motors with initial fluorescence intensities close to the maximum observed (Fig. 3) retained similar intensities after stall. Two others that were less bright before stall increased in fluorescence intensity to the same maximum level during stall. This accounts for the observed 23% increase in mean intensity and ~3-fold decrease in standard deviation after stall compared to before stall and suggests that those motors lacking a full complement of stators while rotating recruited a full complement during stall.

DISCUSSION

We show direct evidence that the number of stators bound to the flagellar motor depends on the external load. Fewer stators are bound to the motor at lower loads. Rough extrapolation of the

TABLE 1 Brightness of motor spots in 5 cells driving 1-μm-diameter magnetic beads before stalling and 300 s after stalling

	Brightness (arbitrary units) or % difference				
Parameter	Cell 1	Cell 2	Cell 3	Cell 4	Cell 5
Before stalling	12,309	9,830	10,068	6,401	7,770
300 s after stalling	12,534	11,343	11,326	10,926	11,148
Difference (%)	+1.8	+15.4	+12.5	+70.7	+43

data of Fig. 3 to zero load indicates that the average number of stators under these conditions may be very close to zero. This suggests that zero-load speeds in the *E. coli* flagellar motor may not be independent of stator number as previously reported (10). Rather, with very low average stator numbers at low load, it is possible that any rotating motors found under those conditions contained only a single stator. At medium and high load, many stators are required to generate sufficient motor torque for swimming and swarming across surfaces. In contrast, motors are relatively inefficient at low load (16, 17) and may gain little from the addition of extra stators.

We previously showed that a sufficiently large IMF is necessary to maintain stators in the motor (9). The lack of binding seen with mutant stators (Fig. 3) also suggests that a stator can attach to the motor only if it is able to generate torque or is in the proton-bound conformation (8). The lack of rotation seen in motors with mutant stators is insufficient to explain the lack of binding: our experiments with stalled motors (Fig. 4) showed that motor rotation is not required for stator binding. Indeed, motor stall, which corresponds to the largest torque in our experiments, induced the largest number of bound stators that we observed.

Our observation of reduced stator number at low load is significant for the interpretation of experiments in which torque-speed curves of flagellar motors have been measured by pooling speed measurements from many motors driving different viscous loads but without the measurement of stator numbers (18–20). The reduction in torque at high speed and low load is the consequence of a combination of the torque per stator and the number of stators. If the changes in load and speed are slower than that of stator exchange, torque-speed curves measured on single motors should show similar effects, in which case speed jumps corresponding to stator loss or gain should be observed. This was not reported in a previous torque-speed study (20) in which the time scale was similar to that expected for stator exchange (4). This study, and the recent observation that single-stator torque speed curves in a Na^+-driven chimeric flagellar motor (21) show the characteristic concave-down shape typical of previous torque-speed measurements, indicate at least that this feature is not entirely due to stator exchange.

Our data suggest a possible asymmetry in the load dependence of stator binding between CW- and CCW-locked motors (Fig. 3). CW-locked motors generate lower torque at intermediate load than CCW-locked motors, which display a "knee" in torque-speed curves at this point (14). Our spot brightness data show a similar knee at intermediate load for CCW-locked motors only, consistent with the hypothesis that the magnitude of torque determines stator stability and thus that the knee in torque leads to the knee in spot brightness in CCW-locked motors. However, we note that the slight asymmetry visible in Fig. 3 is close to the limit of experimental uncertainty. We also note that under physiological conditions, the typical CW motor interval is shorter than the average stator dissociation time ($<$1 s compared to ~15 s); stator number is therefore unlikely to change during natural motor switching.

One simple explanation for our observations would be that the magnitude of the torque generated by each stator determines its stability in the motor. This would explain the observed reduction of stator number with reduced ion-motive force, viscous load, and functionality of stator mutants—these factors all share the common feature of reducing the torque generated by each stator. Similarly, it would explain our observation that the stator numbers observed increase with stall, which increases the torque slightly, and the possible asymmetry between CW and CCW-locked motors. A simple conformational change that altered the length of the linker between the cytoplasmic domains of each stator and its point of anchorage to the cell wall could provide mechanosensitivity, as the free-energy difference between long and short forms would contain a term equal to the length change times the force on a stator, which in turn is proportional to the magnitude of torque generated by that stator. For this mechanism to work, the conformational change in the periplasmic domain of MotB would need to be coupled to other conformational changes that have been observed in MotB during stator binding (21, 22). Investigation of the mechanical role of this domain, perhaps using MotB variants with mutant periplasmic regions, would provide a useful test of this model. Alternatively, more complicated mechanisms involving conformational changes in other motor components, sensitive to the change in stator-rotor interface caused by external load, could also be imagined. FliL is required for correct motor function in several bacterial species, with some Δ*fliL* mutants being able to swim but unable to swarm (23) and some losing motility entirely (24). FliL is an integral motor protein, but the exact nature of the interactions between it and the rest of the flagellar motor is unclear. Furthermore, these interactions may differ substantially between different species. A mechanosensory role for the stators, perhaps aided or enhanced by FliL, would explain the results from this study.

TABLE 2 List of strains used in this study

Strain name	Description	Background (reference)
JPA804	*Egfp-motB*, *fliC*st	RP437 (28)
JPA806	*egfp-motB*, *fliC*st, Δ*cheY*	RP437
JPA807	*egfp-motB* D32A, *fliC*st, Δ*cheY*	RP437
JPA808	*egfp-motB*, *fliC*^{S219C}	HCB1688 (29)

MATERIALS AND METHODS

Strains and cultures. Four experimental *E. coli* strains were used in this study (see Table 2). Cells were grown aerobically with shaking at 30°C in tryptone broth (10 g liter^{-1} Bacto-tryptone, 5 g liter^{-1} sodium chloride) to mid-logarithmic phase (approximate optical density at 600 nm [OD_{600}] of 0.6). Plasmid pIND-CheY**, when used to complement Δ*cheY* strains, was induced with IPTG (isopropyl-β-D-thiogalactopyranoside) to a final concentration of 10 μM.

Experimental procedure. Fluorescence and motility measurements were taken in *E. coli* motility buffer (10 mM potassium phosphate, 1 mM EDTA). Ficoll solutions, when used, were made from a stock solution of Ficoll 400 (GE Healthcare) diluted with motility buffer to the desired concentration. All concentrations are expressed in wt/vol.

In experiments using polystyrene beads (Sigma-Aldrich), JPA806 cells were stuck to glass coverslips and beads attached to flagellar filament stubs by their mutant "sticky" FliCst flagellar filaments as described previously (25). Ficoll solution was added as a final wash-through step in experiments with viscous media. In experiments where magnetic fields were used to stall flagellar motors, JPA808 cells were treated with maleimide-polyethylene glycol 2 (PEG2)-biotin to biotinylate the filament before they were bound to coverslips in tunnel slides using polylysine as described in reference 13. Magnetic S_IO_2 streptavidin-coated beads (Thermo Scientific) (1-μm diameter) were then washed through the tunnel, binding to the biotinylated filaments.

A home-built microscope was used for fluorescence measurements as

described previously (4). In experiments with polystyrene beads, exposure time and illumination intensity were kept constant at 40 ms and 0.12 μW μm^{-2}, respectively. Experiments with magnetic beads used an illumination intensity of 0.08 μW μm^{-2}. A 1,064-nm laser and quadrant photodiode were added to the microscope to allow measurement of motor speed through back focal-plane interferometry as described in reference 25. A sampling rate of 1,000 Hz was used. For stalling experiments, two permanent magnets were installed on the experimental apparatus (one each on the two sides), inducing a linear magnetic field of 20 to 30 mT parallel to the coverslip.

Data analysis. Motor speed was calculated using power spectra of combined (x, y) data as described in reference 26. Data windows of 1 s, beginning at intervals of 0.1 s,were used. All motor speeds given are means of measurements taken over 5 s.

Relative loads for different bead sizes and viscosities were estimated by calculating the viscous drag on the bead for each combination of bead size and Ficoll concentration. Eccentrically rotating beads have a drag coefficient given by $f = 8\pi r_b^2 + 6\pi\eta r_b r_e^2$, where η is viscosity, r_b is bead radius, and r_e is eccentricity (18, 27). Average eccentricities of 1-μm-diameter and 0.35-μm-diameter beads were estimated as 0.2 μm and 0.15 μm, respectively, and correcting factors were applied to account for filament stub drag following Inoue et al. (19). Viscosity values for Ficoll solutions were taken from reference 20.

Fluorescent spot intensity during both steady rotation and stall events was calculated as described previously (4, 9). Briefly, a single image was taken of a cell with a rotating bead. Spot intensity was calculated by subtracting estimated background intensity, individually calculated for each cell by averaging parts of the cell with no motors, from the intensity of regions of interest centered on motor spots and then averaging over the spot region of interest. For stalling experiments, 50 to 100 frame videos of the fluorescent spots were recorded. Photobleaching was accounted for by applying a correcting factor to the fluorescence intensities as described in reference 4. The time constant for photobleaching of GFP-MotB molecules in functioning motors under the conditions of the stalling experiments was found to be $t_0 = 3.06 \pm 0.86$ s. This was calculated from 9 traces of JPA804 cells using the same conditions as used for the stalling experiments.

ACKNOWLEDGMENTS

We thank Howard Berg (Harvard University, Cambridge, MA) for the gift of strain HCB1655.

N.J.D., R.M.B., and J.P.A. were supported by the BBSRC. M.J.T. was supported by EPA Cephalosporin Fund. R.L. was supported by the Human Resource Fund Scholarship Scheme of the Government of Brunei.

REFERENCES

1. **Wadhams GH, Armitage JP.** 2004. Making sense of it all: bacterial chemotaxis. Nat. Rev. Mol. Cell Biol. **5:**1024–1037.
2. **Harshey RM.** 2003. Bacterial motility on a surface: many ways to a common goal. Annu. Rev. Microbiol. **57:**249–273.
3. **Terashima H, Kojima S, Homma M.** 2008. Flagellar motility in bacteria: structure and function of flagellar motor. Int. Rev. Cell Mol. Biol. **279:** 39–85.
4. **Leake MC, Chandler JH, Wadhams GH, Bai F, Berry RM, Armitage JP.** 2006. Stoichiometry and turnover in single, functioning membrane protein complexes. Nature **443:**355–358.
5. **Delalez NJ, Wadhams GH, Rosser G, Xue Q, Brown MT, Dobbie IM, Berry RM, Leake MC, Armitage JP.** 2010. Signal-dependent turnover of the bacterial flagellar switch protein FliM. Proc. Natl. Acad. Sci. U. S. A. **107:**11347–11351.
6. **Yuan J, Branch RW, Hosu BG, Berg HC.** 2012. Adaptation at the output of the chemotaxis signalling pathway. Nature **484:**233–236.
7. **Sowa Y, Berry RM.** 2008. Bacterial flagellar motor. Q. Rev. Biophys. **41:**103–132.
8. **Kojima S, Imada K, Sakuma M, Sudo Y, Kojima C, Minamino T, Homma M, Namba K.** 2009. Stator assembly and activation mechanism of the flagellar motor by the periplasmic region of MotB. Mol. Microbiol. **73:**710–718.
9. **Tipping MJ, Steel BC, Delalez NJ, Berry RM, Armitage JP.** 2012. Quantification of flagellar motor stator dynamics through in vivo proton motive force control. Mol. Microbiol. **87:**338–347.
10. **Yuan J, Berg HC.** 2008. Resurrection of the flagellar rotary motor near zero load. Proc. Natl. Acad. Sci. U. S. A. **105:**1182–1185.
11. **Gabel CV, Berg HC.** 2003. The speed of the flagellar rotary motor of *Escherichia coli* varies linearly with protonmotive force. Proc. Natl. Acad. Sci. U. S. A. **100:**8748–8751.
12. **Kojima S, Blair DF.** 2001. Conformational change in the stator of the bacterial flagellar motor. Biochemistry **40:**13041–13050.
13. **Fukuoka H, Wada T, Kojima S, Ishijima A, Homma M.** 2009. Sodium-dependent dynamic assembly of membrane complexes in sodium-driven flagellar motors. Mol. Microbiol. **71:**825–835.
14. **Yuan J, Fahrner KA, Turner L, Berg HC.** 2010. Asymmetry in the clockwise and counterclockwise rotation of the bacterial flagellar motor. Proc. Natl. Acad. Sci. U. S. A. **107:**12846–12849.
15. **Scharf BE, Fahrner KA, Turner L, Berg HC.** 1998. Control of direction of flagellar rotation in bacterial chemotaxis. Proc. Natl. Acad. Sci. U. S. A. **95:**201–206.
16. **Lo CJ, Leake MC, Pilizota T, Berry RM.** 2007. Nonequivalence of membrane voltage and ion-gradient as driving forces for the bacterial flagellar motor at low load. Biophys. J. **93:**294–302.
17. **Xing J, Bai F, Berry R, Oster G.** 2006. Torque-speed relationship of the bacterial flagellar motor. Proc. Natl. Acad. Sci. U. S. A. **103:**1260–1265.
18. **Sowa Y, Hotta H, Homma M, Ishijima A.** 2003. Torque-speed relationship of the Na+-driven flagellar motor of *Vibrio alginolyticus*. J. Mol. Biol. **327:**1043–1051.
19. **Inoue Y, Lo CJ, Fukuoka H, Takahashi H, Sowa Y, Pilizota T, Wadhams GH, Homma M, Berry RM, Ishijima A.** 2008. Torque-speed relationships of Na+-driven chimeric flagellar motors in *Escherichia coli*. J. Mol. Biol. **376:**1251–1259.
20. **Chen X, Berg HC.** 2000. Torque-speed relationship of the flagellar rotary motor of *Escherichia coli*. Biophys. J. **78:**1036–1041.
21. **Lo CJ, Sowa Y, Pilizota T, Berry RM.** 2013. Mechanism and kinetics of a sodium-driven bacterial flagellar motor. Proc. Natl. Acad. Sci. U. S. A. **110:**E2544–E2551.
22. **Hosking ER, Vogt C, Bakker EP, Manson MD.** 2006. The *Escherichia coli* MotAB proton channel unplugged. J. Mol. Biol. **364:**921–937.
23. **Raha M, Sockett H, Macnab RM.** 1994. Characterization of the fliL gene in the flagellar regulon of *Escherichia coli* and *Salmonella typhimurium*. J. Bacteriol. **176:**2308–2311.
24. **Jenal U, White J, Shapiro L.** 1994. *Caulobacter* flagellar function, but not assembly, requires FliL, a non-polarly localized membrane protein present in all cell types. J. Mol. Biol. **243:**227–244.
25. **Rowe AD, Leake MC, Morgan H, Berry RM.** 2003. Rapid rotation of micron and submicron dielectric particles measured using optical tweezers. J. Mod. Opt. **50:**1539–1554.
26. **Sowa Y, Rowe AD, Leake MC, Yakushi T, Homma M, Ishijima A, Berry RM.** 2005. Direct observation of steps in rotation of the bacterial flagellar motor. Nature **437:**916–919.
27. **Reid SW, Leake MC, Chandler JH, Lo CJ, Armitage JP, Berry RM.** 2006. The maximum number of torque-generating units in the flagellar motor of *Escherichia coli* is at least 11. Proc. Natl. Acad. Sci. U. S. A. **103:** 8066–8071.
28. **Parkinson JS.** 1978. Complementation analysis and deletion mapping of *Escherichia coli* mutants defective in chemotaxis. J. Bacteriol. **135:**45–53.
29. **Turner L, Stern AS, Berg HC.** 2012. Growth of flagellar filaments of *Escherichia coli* is independent of filament length. J. Bacteriol. **194:** 2437–2442.